Current Density Analysis of Electron Transport through Molecular Wires in Open Quantum Systems

Daijiro Nozaki* and Wolf Gero Schmidt

The current density in molecular wires connected to contacts is investigated within the nonequilibrium Green's function formalism combined with the Landauer approach. Energy-dependent and total current density through a series of molecular junctions are calculated in real space representation. A rich variety of current patterns including pronounced ring currents ("vortices") are found even in the defect-free minimal building blocks of molecular devices. The influences of contact positions, functional groups as well as atomic defects on the transport properties are examined systematically for prototypical ortho-, meta-, and para-substituted benzenes as well as heteroaromatic systems. It is found that substitutional functional groups mainly shift the molecular levels and retain characteristic transport channels, while a significant change of electronic pathways and conductance is induced by hetero-aromaticity. The current distribution is used to calculate the static magnetic field distribution in the carbon-based conductors. © 2017 Wiley Periodicals, Inc.

DOI: 10.1002/jcc.24812

Introduction

There has been much progress in the understanding of electron transport through molecular devices and nanostructures.[1,2] Primarily, the transmission properties and I–V characteristics of systems connected to electric contacts were studied in terms of local molecular structures and topologies as well as electron transfer (ET) pathways.[3–6] More recently also the current distribution inside the molecules or nanostructures was explored.[7–15] Electronic pathways in molecules could be identified using inelastic tunneling spectroscopy.[16] Two-dimensional electron gases such as formed in semiconductor heterostructures as well as graphene-related materials are the typical models for theoretical[17–19] and experimental transport studies.[20,21] While scanning tunneling probes give access to the local density of states, their applicability to molecular devices is limited: On the one hand, not all molecular positions may be accessible to the the STM tip. On the other hand, the STM itself may influence the current distribution in the molecule.[22] This underlines the importance of numerical simulations in the exploration of spatially resolved transport characteristics.

The purpose of elucidating the relationship between current density and atomic structures is two-fold. On the one hand, it is expected to assist the device design toward miniaturization, energy saving, and speed by pointing out structural motifs that are prone to problems such as local heating[23–26] or electromigration.[27,28] One the other hand, the current density analysis may give insight into the structure–function relationship, for example, in biological systems such as proteins and enzymes.

In this study, benzenes with different contact positions, with functional groups, and with defects are used as model systems to explore systematically structural and chemical influences on the current distribution. The energy dependent and energy independent local currents are studied using the nonequilibrium Green's function formalism in real-space representation. It is found that the local currents and the current-induced magnetic fields vary in strength and direction depending on local atomic structure and energy. Flow vortices within and outside the molecular structures may occur even in pristine systems, without defects and disorder.

Methodology

We start from the Hamiltonian of the molecule connected to electric contacts via linkers given by $H=H_{\mathrm{M}}+\Sigma_{\mathrm{L}}(E)+\Sigma_{\mathrm{R}}(E)$, where H_{M} describes the molecule and the linkers in the scattering region and $\Sigma_{\mathrm{L/R}}(E)$ are the self-energy terms for the respective left and right contacts.[2] The Hamiltonian H_{M} is defined as $H_{\mathrm{M}}=\sum_i \varepsilon_i c_i^{\dagger} c_i+\sum_{i\neq j} V_{ij} c_i^{\dagger} c_j$, where ε_i is the on-site energy of ith orbital and V_{ij} is the transfer integral between ith and jth orbital. The $c_i^{\dagger}$ and c_i are creation and annihilation operator at the ith site, respectively. Parts of the left and right linkers (parenthesized in Figs. 1a–1c) are included into the scattering region to account for the rearrangement of atoms and charge on contacting the molecule. The retarded (advanced) Green's function $G^{r/a}(E)=[(E\pm i\delta)I-H_{\mathrm{M}}-\Sigma_{\mathrm{L}}-\Sigma_{\mathrm{R}}]^{-1}$ together with the spectral function of the left/right contact $\Gamma_{\mathrm{L/R}}(E)\equiv i[\Sigma_{\mathrm{L/R}}(E)-\Sigma_{\mathrm{L/R}}^{\dagger}(E)]$ allow for calculating the transmission T using the Fisher–Lee relation, that is, $T(E)=\mathrm{trace}[\Gamma_{\mathrm{L}}G^{a}(E)\Gamma_{\mathrm{R}}G^{a}(E)]$.

For calculating the current density through open quantum systems we follow Refs. 7–10. In short, the lesser Green's function is given by

D. Nozaki, W. G. Schmidt
Lehrstuhl für Theoretische Materialphysik, Universität Paderborn, Warburger Str. 100, Paderborn 33098, Germany E-mail: daijiro.nozaki@upb.de
Contract grant sponsor: DFG; Contract grant numbers: FOR1700, FOR1405; Contract grant sponsors: High-performance computer time by the Paderborn Center for Parallel Computing (PC^2) and the HLRS Stuttgart

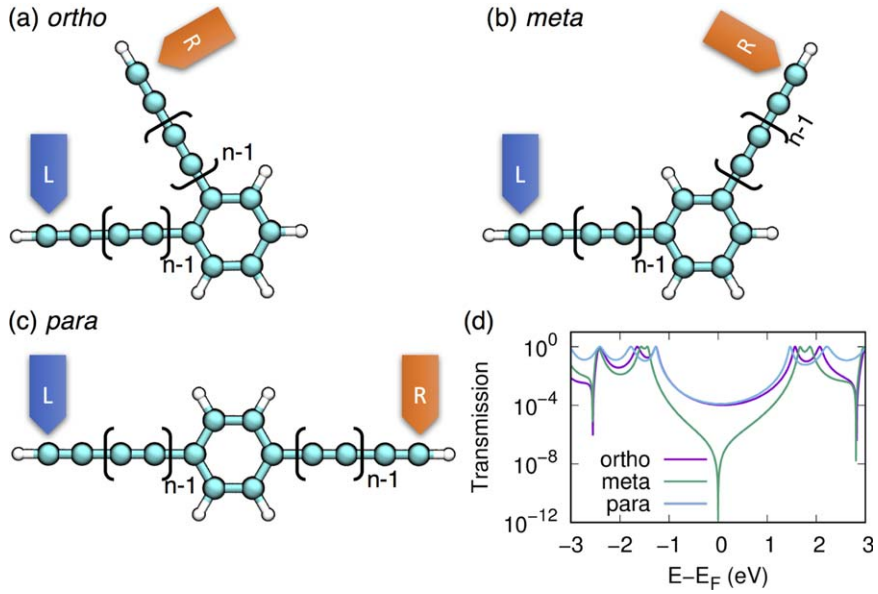

Figure 1. Schematic view of model systems used for the analysis of the local current: *Ortho-, meta-,* and *para*-substituted phenyl rings with linkers (polyene oligomers) are shown in (a–c). Featureless contacts with $\Gamma = 1.0$ eV are attached to the p_z orbital of terminal carbon atoms of the linkers. The length of carbene oligomers is $n = 4$. d) Transmission spectra for the models (a–c) calculated within the wide-band limit (WBL). An antiresonance arising from quantum interference is seen in the middle of the energy gap for *meta*-substituted benzene, chosen here as Fermi energy. [Color figure can be viewed at wileyonlinelibrary.com]

$$G^{<}(E) = iG^{r}(E)[f_L(E)\Gamma_L + f_R(E)\Gamma_R]G^{a}(E), \quad (1)$$

where $f_{L/R}(E)$ are the Fermi distribution function of the left/right contacts defined as $f_{L/R}(E) = 1/[1+\exp(\frac{E-\mu_{L/R}}{k_B T})]$. Here, $\mu_{L/R}$, T, k_B are the chemical potential of the left/right contacts, temperature, and the Boltzmann constant, respectively. For a discussion of the real-space expansion of local currents, see, for example, Refs. 2,7–10. The real space representation of $G^{<}(E)$ may be expanded in atomic orbitals $\{\phi(\vec{r})\}$ as

$$G^{<}(E, \boldsymbol{r}, \boldsymbol{r}') = \sum_{i,j} \phi_i(\boldsymbol{r}) G^{<}_{i,j}(E) \phi_j(\boldsymbol{r}')^{*}. \quad (2)$$

In the absence of the external magnetic field, the current density is given by[29]

$$\boldsymbol{J} = \frac{e}{2m}(\Psi[\boldsymbol{p}\Psi]^{*} + \Psi^{*}[\boldsymbol{p}\Psi]), \quad (3)$$

which can be written in the form

$$\boldsymbol{J}(\boldsymbol{r}; E) = \frac{e}{2m} \lim_{\boldsymbol{r}' \to \boldsymbol{r}} [(\boldsymbol{p} - \boldsymbol{p}')\Psi(\boldsymbol{r})\Psi^{*}(\boldsymbol{r}')], \quad (4)$$

where $\boldsymbol{p} \equiv -i\hbar\nabla$ and $\boldsymbol{p}' \equiv -i\hbar\nabla'$. Here, the gradient operators ∇ and ∇' operate on $\boldsymbol{r}$ and $\boldsymbol{r}'$, respectively. Finally, we replace $\Psi(\boldsymbol{r})\Psi^{*}(\boldsymbol{r}')$ with $-iG^{<}(E, \boldsymbol{r}, \boldsymbol{r}')/2\pi$ to obtain the energy-dependent current density

$$2\pi \boldsymbol{J}(\boldsymbol{r}; E) = -\frac{e\hbar}{2m} \lim_{\boldsymbol{r}' \to \boldsymbol{r}} [(\nabla - \nabla')G^{<}(\boldsymbol{r}, \boldsymbol{r}'; E)]. \quad (5)$$

The total current density is given by energy integration,

$$\boldsymbol{J}(\boldsymbol{r}) = 2\int \boldsymbol{J}(\boldsymbol{r}; E) dE, \quad (6)$$

where the factor 2 accounts for spin degeneracy.

Numerically, our calculations are performed using the density functional-based tight binding (DFTB) method as implemented in the DFTB+ package[30] together with the pbc-0-3 basis set.[31] At first, the central molecules and linkers were separately structurally relaxed. Thereby polyene oligomers having four units were used as conducting linkers. Next, these linkers were attached to the central molecule and the complete structure was relaxed again. In the third step, fictitious contacts approximated within the wide band limit (WBL) were attached to the terminal p_z orbitals of the two linkers (see Fig. 1) and the current density was calculated as described above. The electronic temperature and the bias voltages are set to 300 K and 0.5 V, respectively, for all calculations. This means that the chemical potential for the left (right) featureless contact is shifted up (down) by 0.25 eV corresponding to a total bias of 0.5 V. The bias dependence of the retarded Green's function is not included here for simplicity.

Obviously, the accuracy of the numerical results used here to illustrate our approach depends on the level of theory used for the underlying electronic structure calculation. It can be improved, for example, by including quasiparticle effects in the electronic self-energies:[32–39] The same framework can then be used, but the eigenenergies and eigenstates $\{\varepsilon_i^{KS}, \Psi_i^{KS}\}$ are to be replaced by the corresponding quasi-particle quantities $\{\varepsilon_i^{QP}, \Psi_i^{QP}\}$. This will shift the resonance peaks in the transmission and thus modify the current.

Results and Discussion

Local current through benzenes with different contact positions

Benzene and its derivatives substituted at *ortho*, *meta*, and *para* positions (cf. Fig. 1) are common test-beds for electron

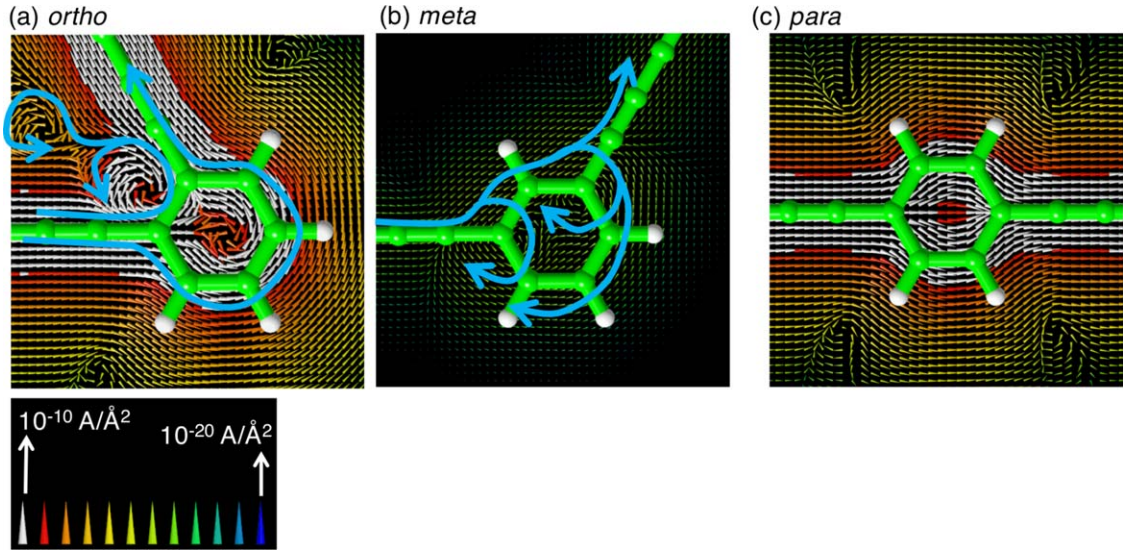

Figure 2. Electron current density in benzenes with different contacts positions. A 2D slice of the 3D electronic current vector field 1.0 Å below the molecular plane is plotted. The chemical potential for the left (right) featureless contact is shifted up (down) by 0.25 eV. The energy-dependent current density is shown in Supporting Information Figures S1–S3. The vortices observed in the energy-dependent current density in Supporting Information Figures S1–S3 still remain even after energy integration. [Color figure can be viewed at wileyonlinelibrary.com]

transport studies. Especially, *meta*-substituted benzene is known to exhibit an antiresonance for mid-gap energy due to quantum interference, see, for example, Refs. 3,5,7,14,22,40–45. While the bond current through the benzene and its derivatives has been studied, this does not hold for its spatial distribution. In Figure 2, the current distribution according to eq. (6) is shown for benzenes with different contact positions. The energy-dependent contributions to these currents [eq. (5)] are shown in the Supporting Information, in Figures S1–S3. They depend strongly on contact position and energy. The rotation direction of the electronic vortex flips when passing the antiresonance energy in *meta*-substituted benzene (see Supporting Information Figs. S2b-S2c). Some vortices present in the energy-dependent current density remain after the energy integration in eq. (6) and are still visible in the total current density, as indicated by arrows in Figures 2a and 2b. Therefore, current-induced magnetic fields can be expected, as will be explored below. The occurrence of current vortices is not limited to intramolecular regions, they are also observed outside the molecule, see, for example, Figures 2a and 2c. In case of *meta*-substitution, the centers of vortices are localized not on the top of the center of the phenyl ring like in Figure 2a, but on the top of carbon atoms where electric leads are attached, cf. Figure 2b.

Influence of functional groups

The electronic structures and transport properties of organic materials are frequently modified and tuned by means of attaching functional groups.[14,15,46–59] Here, the influence of functional groups is exemplarily studied using benzenes connected to electric leads at the *para* position. In Figure 3, the current distribution according to eq. (6) is shown for the molecular wires with different functional groups (X=—H, —CH_3, —COOH, —NH_2, —NO_2, and —OH). It can be seen that all functional groups substituting for hydrogen give rise to vortices outside the phenyl ring. The respective net contribution of upper, that is, functionalized, and lower part of the molecular structure to the total current through the molecule is shown in Figure 3g. As expected, upper and lower pathway contribute equally in case of the pristine system (X= —H in Fig. 3a) in accordance with the molecular symmetry. The symmetry break induced by the functional groups, however, clearly shows up in the current distribution. The lower current flow is higher than the upper one—most pronounced for the —OH group—for all cases except for the one with —COOH group. These findings can partially be understood from the on-site energies of the p_z orbitals along the upper and lower pathways, see Figures 4g–4h. All samples apart from the one with —COOH group have shallower potential wells in the lower pathways than in the upper pathways. The —OH group, for example, is found to induce a strong corrugation in the upper energy profile that can be expected to give rise to potential well scattering,[60] while no significant differences are observed for the —COOH group. The hydroxyl group discussed above is found to lead to the strongest variation, 26%, in the relative current strengths through upper and lower molecular bridge. Generally, the modifications are moderate, as also shown by the rather similar isosurfaces of the respective current densities shown in Figures 4a–4f. This is due to the transport channel defined by the carbon atoms that is not affected by the functionalization, at least not for energies close to the Fermi energy, see Figure 3h. The functional groups shift only the relative positions of molecular eigenstates with respect to the Fermi energy by donating or withdrawing electrons, and do not substantially change the electronic structure along the pathways. Similar trends were observed earlier.[15] Also, it is known that the *meta*-substitution is particularly sensitive to the change of the functional group[14,53] and the change of the position of the Fermi energy. This agrees with the present

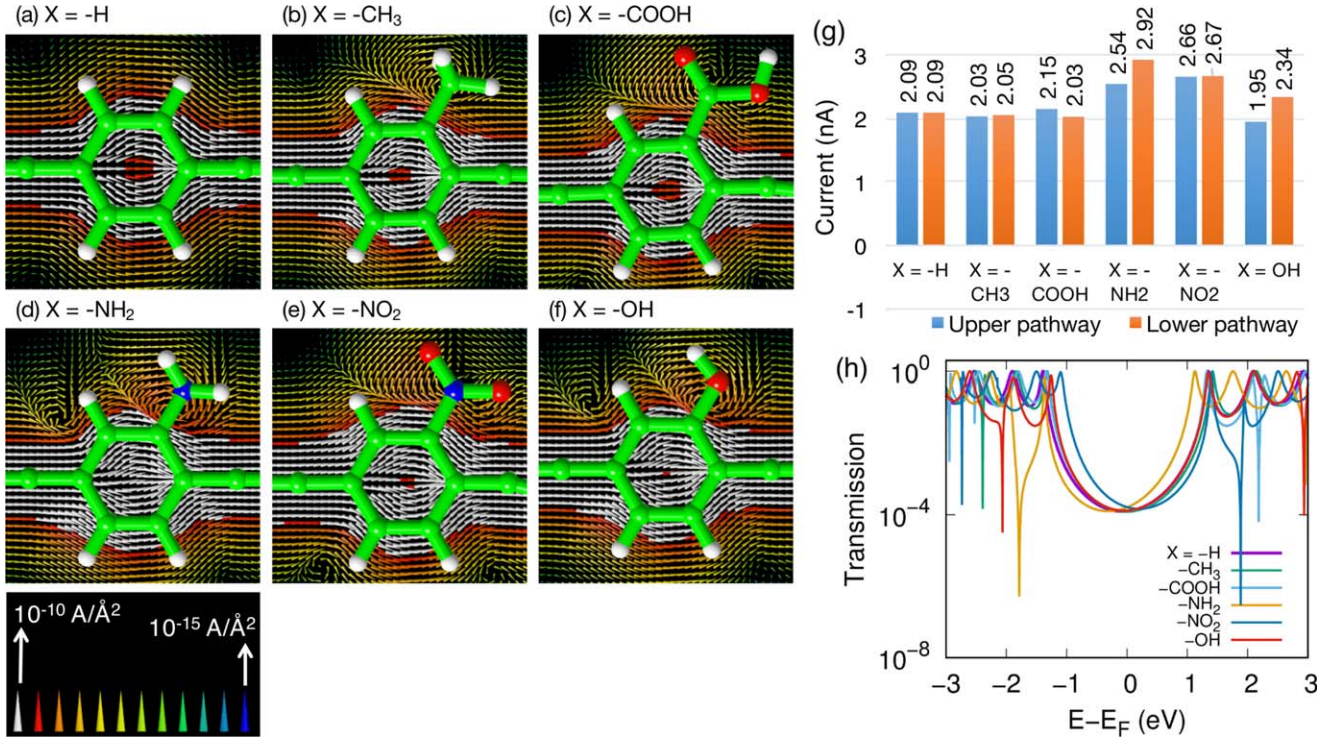

Figure 3. a–f) Electron current density in *para*-substituted benzene with different functional groups plotted in a plane 1.0 Å beneath the molecule. The parameters for broadening function within WBL are set to $\Gamma_{L/R}=1.0$ eV. The chemical potential for the left (right) featureless contact is shifted up (down) by 0.25 eV. Current vortices appear around the functional groups. Major pathways through the benzene frameworks are hardly disturbed by the functional groups (see also Figs. 4a–4f). g) Comparison of currents through upper and lower pathways in a series of the benzene derivatives and (h) their transmission spectra. [Color figure can be viewed at wileyonlinelibrary.com]

analysis of the local current in real-space representation (see Supporting Information Figs. S6 and S7). The details of the influence of the bias voltage and the position of the Fermi energies are summarized in Supporting Information Figures S4–S9.

Influence of defects and impurities

Conducting organic materials such π-conjugated oligomers and polymers typically contain various defects arising from disorder and impurities which modify the transfer integrals and substantially impact the transport properties.[50,61–67] Walz et al. have

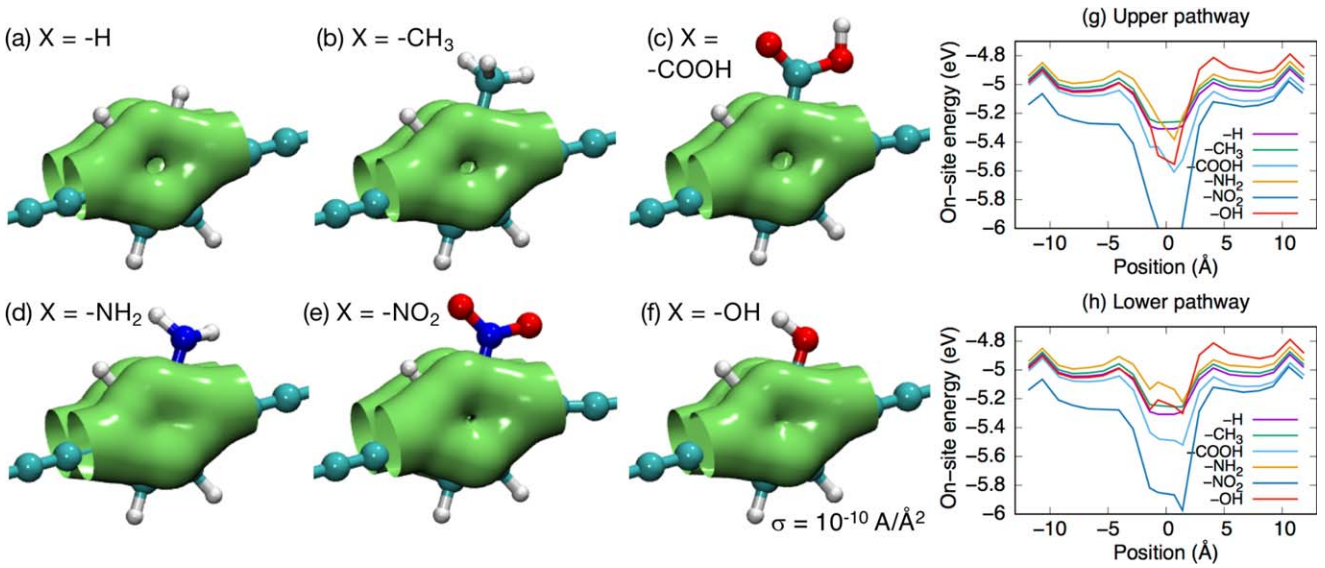

Figure 4. a–f) Isosurface of local current density for the benzene derivatives with functional groups. g, h) On-site energies of p_z orbitals along the upper and lower pathways. Threshold value for the isosurface of the current density is $\sigma=10^{-10}$A/Å^2. [Color figure can be viewed at wileyonlinelibrary.com]

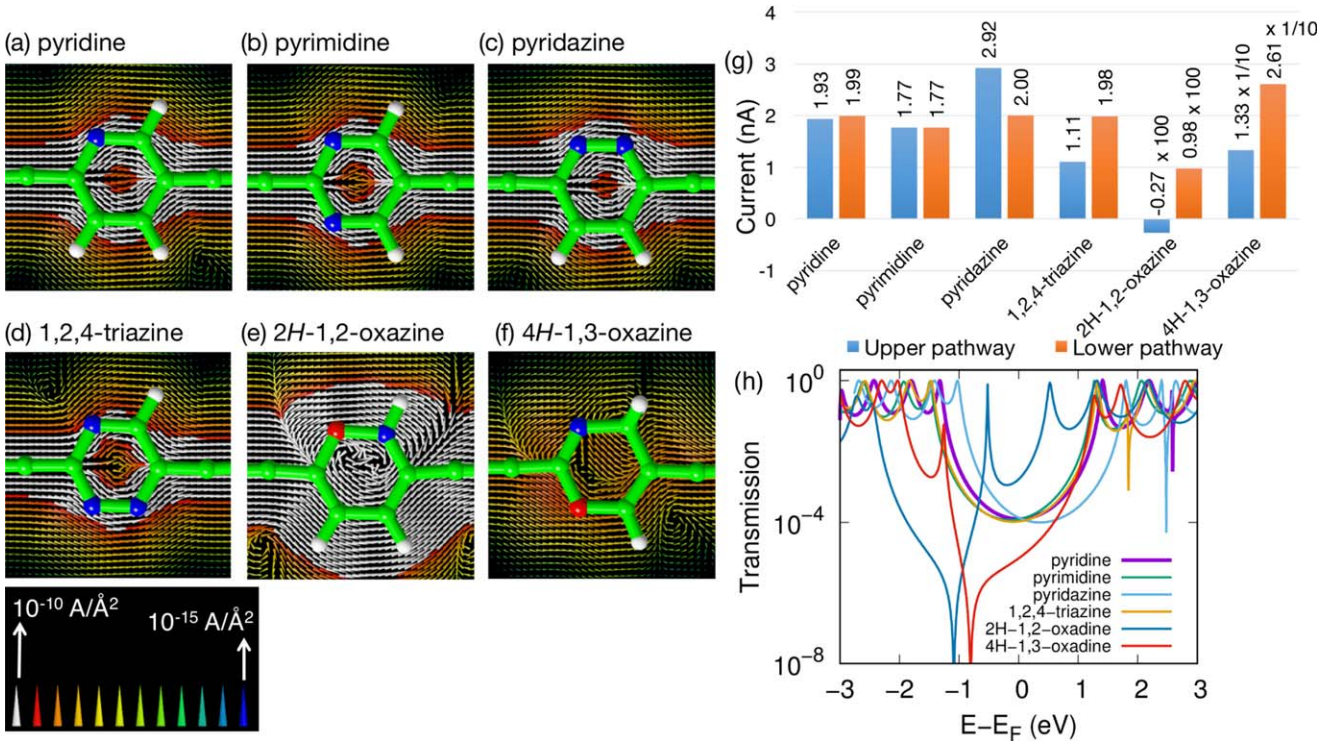

Figure 5. Electron current density in heteroaromatic systems. a–f) A 2D slice of the 3D electronic current vector field 1.0 Å below the molecular plane is plotted. The broadening parameter within the WBL is $\Gamma_{L/R}$=1.0 eV. The chemical potential for the left (top) featureless contact is shifted up (down) by 0.25 eV. g) Comparison of currents through upper and lower pathways in a series of heteroaromatic systems and (h) the calculated transmission spectra. [Color figure can be viewed at wileyonlinelibrary.com]

shown that defects such as adatoms or substitutional nitrogen induce vortices and inhomogeneities in the current density in graphene nanoribbons.[8,9]

Below the influence of oxygen, nitrogen, and hydrogen defects on the current density in *para*-subsitututed benzene systems is studied. Figure 5 summarizes the effect of substitutional defects in the phenyl rings on the current density and the transmission spectra. In comparison to the influence of functional groups, cf. Figure 3, far more drastic changes of the current density (cf. Figs. 6a–6f) are observed. This is attributed to the substantial defect-induced change of the electronic parameters such as on-site energies (see also Figs. 6g–6h) and transfer integrals along the electronic pathways (see also Supporting Information Fig. S10). The oxygen-related defects shown in Figures 5e and 5f even cause an electronic back flow. The interpretation of the current density changes only in

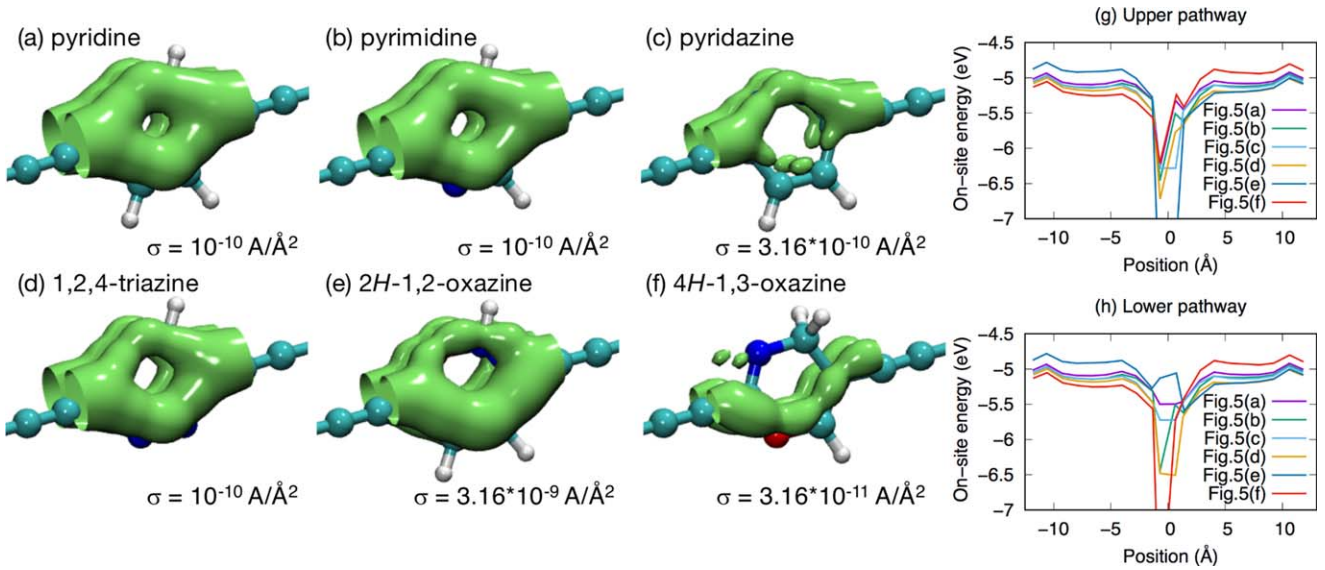

Figure 6. a–f) Isosurface of local current density for the benzene derivatives with different defects. g–h) On-site energies of p_z orbitals along the upper and lower pathways. σ is the threshold value for the isosurface of the current density. [Color figure can be viewed at wileyonlinelibrary.com]

Table 1. Comparison of current (in nA) obtained either from the integration of the current density over a cross-sectional area normal to the current flow (A) or from the energy integral of the transmission function over the bias window (B).

Functional group	—H	—CH_3	—COOH	—NH_2	—NO_2	—OH
System	Figure 3a	Figure 3b	Figure 3c	Figure 3d	Figure 3e	Figure 3f
A	4.09	4.08	4.18	5.46	5.33	4.29
B	5.16	4.98	5.28	6.80	6.88	5.34
System	Figure 5a	Figure 5b	Figure 5c	Figure 5d	Figure 5e	Figure 5f
A	3.92	3.54	4.92	3.09	71.0	0.394
B	5.09	5.05	5.88	4.33	98.0	0.417

terms of modified on-site energies—successful for the functional groups above—fails for some substitutional defects: The lower electron pathway of the structure Figure 5f, for example, features a deep potential well (cf. Figs. 6g and 6h). Nevertheless it carries about twice as much current as the upper pathway, cf. Figure 5g. This indicates strong modifications of the transfer integrals. The transmission calculated for the defect structures studied here varies largely and within a wide energy window, cf. Figure 5h. Interestingly, the oxazine derivatives shown in Figures 5e and 5f give rise to antiresonances in the transmission spectra. In case of 4*H*-1,3-oxazine (Fig. 5f) the antiresonance nearly quenches the current, while, counterintuitively, the current is even enhanced for 2*H*-1,2-oxazine (Fig. 5e). The latter results from the molecular level shift caused by the substitutional defects, which shift the antiresonance in the transmission spectrum away from the Fermi energy.

Finally, we compare the current calculated, on the one hand, using the conductance spectra (i.e., transmission function), and, on the other hand, from the present current densities. The results for the systems in Figures 3 and 5 are summarized in Table 1. Here, the current density was integrated over a cross-sectional area normal to the current flow or an energy integration of the transmission function over the bias window, respectively, was performed. It can be seen from Table 1 that the currents obtained from the two approaches agree nicely, with deviations typically smaller than 20%. Both approaches result in the same trends concerning the influence of functional groups (Fig. 3) and defects (Fig. 5). In addition to the information obtained from the transmission profile, however, the analysis of local currents allows for identifying electron pathways and back flows (see e.g., Fig. 5f).

Current-induced magnetic field

Static currents through molecular systems induce magnetic fields.[8,9,68,69] The variety of the patterns in the current density

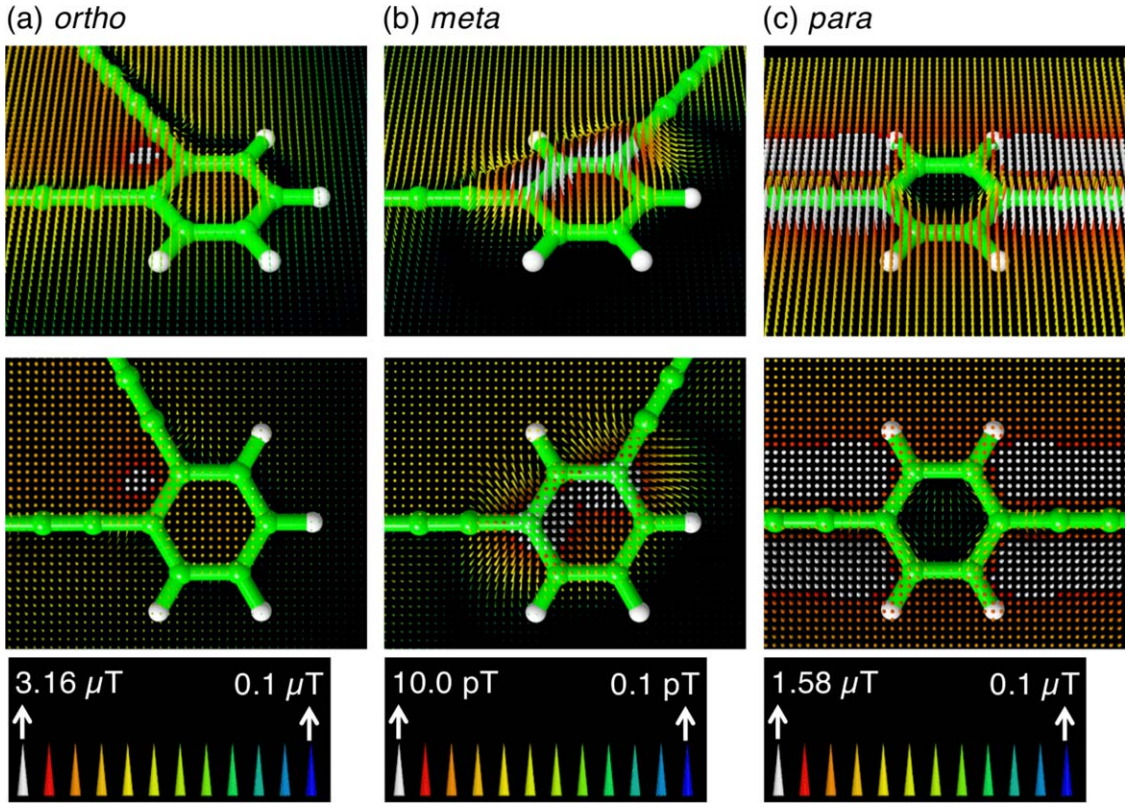

Figure 7. Side and top view of the current-induced magnetic field in (a) *ortho*-, (b) *meta*-, and (c) *para*-subsituted benzenes (current strength an other parameters correspond to Fig. 2). The field is plotted in a plane 0.5 Å above of the molecular plane. [Color figure can be viewed at wileyonlinelibrary.com]

discussed above is expected to cause various patterns in the magnetic field, the control of which may be interesting in the context of high-density molecular memory storage consisting of single molecular magnets.[70–72] In addition, it has been proposed that the NMR-type experiment in the presence of dc-current flow can be performed to observe the spatial fluctuations of the induced magnetic fields.[8] Here, we study exemplarily the influence of the benzene contact positions on the current-induced magnetic field. It is calculated using the Biot–Savart law

$$\boldsymbol{B}(\boldsymbol{r}) = \frac{\mu_0}{4\pi}\int_V \frac{\boldsymbol{J}\times\hat{\boldsymbol{r}}'\,dV}{|\boldsymbol{r}'|^2}, \tag{7}$$

where dV is the volume element, $\boldsymbol{J}$ is the current density in that volume, μ_0 is the vacuum permeability, and $\boldsymbol{r}'$ is the unit vector from the volume element to the point $\boldsymbol{r}$ at which the field is being computed.

The calculated magnetic field for the differently contacted benzenes are shown in Figure 7. It summarizes the current-induced magnetic fields in three configurations with different contact positions. The corresponding current densities are shown in Figure 2. In case of the *ortho*-substitution, several current vortices appear inside and outside the phenyl ring (see Fig. 2a), thus magnetic flux generated from these current vortices is expected. This is indeed the case, as shown in Figure 7a. The signatures of the strongest current vortices inside and outside the phenyl ring are clearly visible by the magnetic flux penetrating through the molecular plane. Interestingly, the maximum of the magnetic field is not inside, but outside the phenyl ring, due to the high current density at the contacts, as well as due to the cancellation of the magnetic fields induced by the partially parallel current around the phenyl ring (see Fig. 2a). *Meta*-substituted benzene features an antiresonance in the electron transmission spectrum near the Fermi energy. Hence, the current density and consequently the current-induced magnetic field is weaker than for the *ortho*-substitution. Again, the magnetic field is strongest close to the carbon atoms where electric contacts are attached. There strong current vortices form as shown in Figure 2b. It is also noteworthy that the sign of the magnetic field is opposite to the case of *ortho*-substitution. In case of the *para*-substitution (Fig. 7c), the magnetic fields induced by the two currents along the upper and lower molecular pathways partially cancel each other. Thus, there is nearly no magnetic field inside the phenyl ring.

Conclusions

The current density in benzene-derived molecular structures embedded between electric contacts has been studied from the Green's function formalism combined with the Landauer approach. It is found that the local currents depend strongly on the contact positions, functional substituents, and defects. In cases where functional groups are attached on side of the main electron pathway, the variation of the local currents can largely be interpreted in terms of potential-well scattering. This simple interpretation breaks down in case of substitutional defects in the electron pathway. In this case not only the on-side energies but also the transfer integrals are affected, and very strong modifications of the current density may result. A variety of current vortices form, even outside the molecular structure. This clearly shows, on the one hand, the limits of electron pathway analyses based on bond strengths. On the other hand, the random magnetic fields arising from these vortices in combination with multiple scattering processes can be expected to cause spin relaxation in materials with low spin-orbit interaction, such as organic semiconductors. We expect current density analyses such as performed here to be helpful for the design of functional molecular devices with enhanced performance as well as for the interpretation and elucidation of experimental observations.

Keywords: electron transport · molecular electronics · nanotechnology · quantum chemistry · *ab initio* calculations · local current · current-induced magnetic field

How to cite this article: D. Nozaki, W. G. Schmidt. *J. Comput. Chem.* **2017**, *38*, 1685–1692. DOI: 10.1002/jcc.24812

Additional Supporting Information may be found in the online version of this article.

[1] J. C. Cuevas, E. Scheer, Molecular Electronics: An Introduction to Theory and Experiment; World Scientific: Singapore, **2009**.
[2] S. Datta, Electronic Transport in Mesoscopic Systems; Cambridge University Press: Cambridge, **1995**).
[3] P. Sautet, C. Joachim, *Chem. Phys. Lett.* **1988**, *153*, 511.
[4] T. N. Todorov, *J. Phys. Condens. Matter* **2002**, *14*, 3049.
[5] C. Patoux, C. Coudret, J.-P. Launay, C. Joachim, A. Gourdon, *Inorg. Chem.* **1997**, *36*, 5037.
[6] D. N. Beratan, J. N. Onuchic, J. R. Winkler, H. B. Gray, *Science* **1992**, *258*, 1740.
[7] G. C. Solomon, C. Herrmann, T. Hansen, V. Mujica, M. A. Ratner, *Nat. Chem.* **2010**, *2*, 223.
[8] M. Walz, J. Wilhelm, F. Evers, *Phys. Rev. Lett.* **2014**, *113*, 136602.
[9] J. Wilhelm, M. Walz, F. Evers, *Phys. Rev. B* **2015**, *92*, 014405.
[10] K. Hirose,T. Ono, Y. Fujimoto, S. Tsukamoto, First-Principles Calculationsin Real-Space Formalism, Electronic Configurations and Transport Properties of Nanostructures; Imperial College Press: London, **2005**.
[11] T. Ono, K. Hirose, *Phys. Rev. B* **2004**, *70*, 033403.
[12] T. Ono, K. Hirose, *Phys. Rev. Lett.* **2007**, *98*, 026804.
[13] M. Otani, T. Ono, K. Hirose, *Phys. Rev. B* **2004**, *69*, 121408.
[14] C. Herrmann, G. C. Solomon, M. A. Ratner, *J. Chem. Phys.* **2011**, *134*, 224306.
[15] H. Schlicke, C. Hermann, *ChemPhysChem* **2014**, *15*, 4011.
[16] A. Troisi, J. M. Beebe, L. B. Picraux, R. D. van Zee, D. R. Stewart, M. A. Ratner, J. G. Kushmerick, *Proc. Natl. Acad. Sci. USA* **2007**, *104*, 14255.
[17] K. Kazymyrenko, X. Waintal, *Phys. Rev. B* **2008**, *77*, 115119.
[18] R. A. Jalabert, W. Szewc, S. Tomsovic, D. Weinmann, *Phys. Rev. Lett.* **2010**, *105*, 166802.
[19] H. Haugen, D. Huertas-Hernando, A. Brataas, X. Waintal, *Phys. Rev. B* **2010**, *81*, 174523.
[20] M. A. Topinka, B. J. LeRoy, S. E. J. Shaw, E. J. Heller, R. M. Westervelt, K. D. Maranowski, A. C. Gossard, *Science* **2000**, *289*, 2323.
[21] M. A. Topinka, B. J. LeRoy, R. M. Westervelt, S. E. J. Shaw, R. Fleischmann, E. J. Heller, K. D. Maranowski, A. C. Gossard, *Nature* **2001**, *410*, 183.
[22] S.-G. Chen, Y. Zhang, S.-K. Koo, H. Tian, C.-Y. Yam, G.-H. Chen, M. A. Ratner, *J. Phys. Chem. Lett.* **2015**, *5*, 2748.
[23] R. Murali, Y. Yang, K. Brenner, T. Beck, J. D. Meindl, *Appl. Phys. Lett.* **2009**, *94*, 243114.

[24] R. Yang, Z. Wang, P. X.-L. Feng, *Nanoscale* **2014**, *6*, 12383.
[25] P. G. Collins, M. S. Arnold, P. Avouris, *Science* **2001**, *292*, 706.
[26] A. Liao, R. Alizadegan, Z.-Y. Ong, S. Dutta, F. Xiong, K. J. Hsia, E. Pop, *Phys. Rev. B* **2010**, *82*, 205406.
[27] S. Hertel, F. Kisslinger, J. Jobst, D. Waldmann, M. Krieger, H. B. Weber, *Appl. Phys. Lett.* **2011**, *98*, 212109.
[28] J. P. Gambino, T. C. Lee, F. Chen, T. D. Sullivan, *Proc. IEEE IPFA* **2009**, 677.
[29] R. P. Feynman, Lectures on Physics, Vol *III*; Addison-Wesley: New York, **1965**; pp. 21–24.
[30] T. Frauenheim, G. Seifert, M. Elstner, Z. Hajnal, G. Jungnickel, F. Porezag, S. Suhai, R. Scholz, *Phys. Status Solidi B* **2000**, *217*, 41.
[31] E. Rauls, R. Gutierrez, J. Elsner, T. Frauenheim, *Solid State Commun.* **1999**, *111*, 459.
[32] L. Hedin, *Phys. Rev.* **1965**, *139*, A796.
[33] K. S. Thygesen, A. Rubio, *Phys. Rev. B* **2008**, *77*, 115333.
[34] D. J. Mowbray, G. Jones, K. S. Thygesen, *J. Chem. Phys.* **2008**, *128*, 111103.
[35] J. P. Bergfield, C. A. Stafford, *Phys. Rev. B* **2009**, *79*, 245125.
[36] J. M. Garcia-Lastra, C. Rostgaard, A. Rubio, K. S. Thygesen, *Phys. Rev. B* **2009**, *80*, 245427.
[37] S. Y. Quek, H. J. Choi, S. G. Louie, J. B. Neaton, *Nano Lett.* **2009**, *9*, 3949.
[38] K. Kaasbjerg, K. S. Thygesen, *Phys. Rev. B* **2010**, *81*, 085102.
[39] J. P. Bergfield, G. C. Solomon, C. A. Stafford, M. A. Ratner, *Nano Lett.* **2011**, *11*, 2759.
[40] S. N. Yaliraki, M. A. Ratner, *Ann. N. Y. Acad. Sci.* **2002**, *960*, 153.
[41] K. Walczak, *Open Chem.* **2004**, *2*, 524.
[42] C. A. Stafford, D. M. Cardamone, S. Mazumdar, *Nanotechnology* **2007**, *18*, 424014.
[43] G. C. Solomon, D. Q. Andrews, T. Hansen, R. H. Goldsmith, M. R. Wasielewski, R. P. Van Duyne, M. A. Ratner, *J. Phys. Chem.* **2008**, *129*, 054701.
[44] T. Hansen, G. C. Solomon, D. Q. Andrews, M. A. Ratner, *J. Chem. Phys.* **2009**, *131*, 194704.
[45] D. A. Lovey, R. H. Romero, *Chem. Phys. Lett.* **2012**, *530*, 86.
[46] J. E. Anthony, *Chem. Rev.* **2006**, *106*, 5028.
[47] R. D. Tomps, *Prog. Phys. Org. Chem.* **1976**, *12*, 1.
[48] C. Hansch, A. Leo, R. W. Taft, *Chem. Rev.* **1991**, *91*, 165.
[49] H. Lissau, R. Frisenda, S. T. Olsen, M. Jevric, C. R. Parker, A. Kadziola, T. Hansen, H. S. J. van der Zant, M. B. Nielsen, K. V. Mikkelsen, *Nat. Commun.* **2015**, *6*, 10233.
[50] C. Cao, A. F. Kemper, L. Agapito, J.-W. Zhang, Y. He, A. Rinzler, H.-P. Cheng, X.-G. Zhang, A. R. Rocha, S. Sanvito, *Phys. Rev. B* **2009**, *79*, 075127.
[51] W.-Y. Lo, W. Bi, L. Li, I. H. Jung, L. Yu, *Nano Lett.* **2015**, *15*, 958.
[52] S. K. Maiti, *Solid State Commun.* **2008**, *145*, 126.
[53] M. C. Garner, G. C. Solomon, M. Strange, *J. Phys. Chem. C* **2016**, *120*, 9097.
[54] T. M. Perrine, R. G. Smith, C. Marsh, B. D. Dunietz, *J. Chem. Phys.* **2008**, *128*, 154706.
[55] L. Venkataraman, Y. S. Park, A. C. Whalley, C. Nuckolls, M. S. Hybertsen, M. L. Steigerwald, *Nano Lett.* **2007**, *7*, 502.
[56] J. Maeng, S. B. Kim, N. J. Lee, E. Choi, S.-Y. Jung, I. Hong, S.-H. Bae, J. T. Oh, B. Lim, J. W. Kim, C. J. Kang, S. Koo, *Chemistry* **2010**, *16*, 7395.
[57] Y. Zhao, S. Lindsay, S. Jeon, H.-J. Kim, L. Su, B. Lim, S. Koo, *Chemistry* **2013**, *19*, 10832.
[58] A. A. Kocherzhenko, L. D. A. Siebbeles, F. C. Grozema, *J. Phys. Chem. Lett.* **2011**, *2*, 1753.
[59] A. C. Aragonès, N. Darwish, J.-O. Im, B. Lim, J. Choi, S. Koo, I. Díez-Pérez, *Chemistry* **2015**, *21*, 7716.
[60] S. Wippermann, N. Koch, W. G. Schmidt, *Phys. Rev. Lett.* **2008**, *100*, 106802.
[61] E. Gracia-Espino, F. López-Urías, H. Terronesd, M. Terronesef, *RSC Adv.* **2016**, *6*, 21954.
[62] D. Orlikowski, M. B. Nardelli, J. Bernholc, C. Roland, *Phys. Rev. B* **2000**, *61*, 14194.
[63] T. Yamamoto, K. Watanabe, *Phys. Rev. Lett.* **2006**, *96*, 255503.
[64] G. P. Zhang, X. Liu, C. Z. Wang, Y. X. Yao, J. Zhang, K. M. Ho, *J. Phys. Condens. Matter* **2013**, *25*, 105302.
[65] G. Lee, K. S. Kim, K. Cho, *J. Phys. Chem. C* **2011**, *115*, 9719.
[66] A. Lücke, W. G. Schmidt, E. Rauls, F. Ortmann, U. Gerstmann, *J. Phys. Chem. B* **2015**, *119*, 6481.
[67] A. Lücke, F. Ortmann, M. Panhans, S. Sanna, E. Rauls, U. Gerstmann, W. G. Schmidt, *J. Phys. Chem. B* **2016**, *120*, 5572.
[68] J. A. Pople, *Mol. Phys.* **1958**, *1*, 175.
[69] M. D. Peeks, T. D. W. Claridge, H. L. Anderson, *Nature* **2017**, *541*, 200.
[70] T. Lis, *Acta Crystallogr. Sect. B* **1980**, *36*, 2042.
[71] A. Caneschi, D. Gatteschi, R. Sessoli, A. L. Barra, L. C. Brunel, M. Guillot, *J. Am. Chem. Soc.* **1991**, *113*, 5873.
[72] S. M. J. Aubin, M. W. Wemple, D. M. Adams, H.-L. Tsai, G. Christou, D. N. Hendrickson, *J. Am. Chem. Soc.* **1996**, *118*, 7746.

Received: 4 January 2017
Revised: 29 March 2017
Accepted: 30 March 2017
Published online on 7 May 2017